DOI: 10.1002/chem.200701802

Is the μ-Oxo-μ-Peroxodiiron Intermediate of a Ribonucleotide Reductase Biomimetic a Possible Oxidant of Epoxidation Reactions?

Sam P. de Visser*[a]

Abstract: Density functional calculations on a μ-oxo-μ-peroxodiiron complex (**1**) with a tetrapodal ligand BPP (BPP = *N*,*N*-bis(2-pyridylmethyl)-3-aminopropionate) are presented that is a biomimetic of the active site region of ribonucleotide reductase (RNR). We have studied all low-lying electronic states and show that it has close-lying broken-shell singlet and undecaplet ($S=0$, 5) ground states with essentially two sextet spin iron atoms. In strongly distorted electronic systems in which the two iron atoms have different spin states, the peroxo group moves considerably out of the plane of the μ-oxodiiron group due to orbital rearrangements. The calculated absorption spectra of ^{1,11}**1** are in good agreement with experimental studies on biomimetics and RNR enzyme systems. Moreover, vibrational shifts in the spectrum due to $^{18}O_2$ substitution of the oxygen atoms in the peroxo group follow similar trends as experimental observations. To identify whether the μ-oxo-μ-1,2-peroxodiiron or the μ-oxo-μ-1,1-peroxodiiron complexes are able to epoxidize substrates, we studied the reactivity patterns versus propene. Generally, the reactions are stepwise via radical intermediates and proceed by two-state reactivity patterns on competing singlet and undecaplet spin state surfaces. However, both the μ-oxo-μ-1,2-peroxodiiron and μ-oxo-μ-1,1-peroxodiiron complex are sluggish oxidants with high epoxidation barriers. The epoxidation barriers for the μ-oxo-μ-1,1-peroxodiiron complex are significantly lower than the ones for the μ-oxo-μ-1,2-peroxodiiron complex but still are too high to be considered for catalytic properties. Thus, theory has ruled out two possible peroxodiiron catalysts as oxidants in RNR enzymes and biomimetics and the quest to find the actual oxidant in the enzyme mechanism continues.

Keywords: density functional calculations · enzyme catalysis · enzyme models · nonheme models · oxygen

Introduction

Many enzymes utilize molecular oxygen on a diiron center for a variety of biochemical functions.[1] As such, there is great interest from the bioinorganic chemistry community to create biomimetics based on the structural motif of these metal centers for use as new and powerful catalysts. A common pattern shared by these enzymes is a carboxylate-bridged diiron center and has been observed, for instance, in hemerythrin (Hr), ribonucleotide reductase (RNR), ferritin, methane monoxygenase (MMO), and Δ^9-stearoyl-acyl carrier protein desaturase (Δ^9D).[2–5] Despite their structural similarities these enzymes have different biochemical functions, that is, Hr is a dioxygen carrier, tyrosynyl radicals are generated in RNR, methane is hydroxylated in MMO, and Δ^9D catalyzes alkane dehydrogenation. Figure 1 shows an exam-

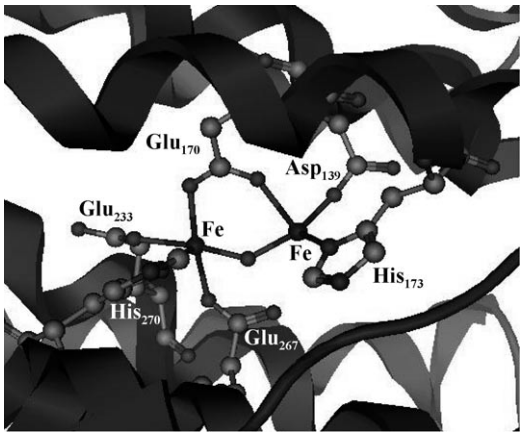

Figure 1. The active site region of mouse RNR from reference [6]. All amino acids are labeled as in the PDB file.

[a] Dr. S. P. de Visser
The Manchester Interdisciplinary Biocenter and
the School of Chemical Engineering and Analytical Science
The University of Manchester
131 Princess Street, Manchester M1 7DN (UK)
Fax: (+44) 161-306-5201
E-mail: sam.devisser@manchester.ac.uk

Supporting information for this article is available on the WWW under http://www.chemeurj.org/ or from the author.

ple of a typical enzyme active site region of mouse RNR with labels taken from the Protein Databank (PDB) file.[6] Thus, the two iron atoms are held in position by interactions with carboxylic acid groups of glutamate or aspartate residues as well as by two histidine side chains. There are two bridging groups between the diiron moiety, namely an oxo group and a carboxylic acid side chain of Glu_{170}. In many nonheme enzymes, iron atoms are held in position by interactions with carboxylic acid groups or histidine groups, and a motif with two-histidines and one-carboxylate group is very common and appears, for instance, in the α-keto acid dioxygenases, a large class of enzymes involved in the biosynthesis of antibiotics as well as DNA base repair.[7,8]

Thus, generally difficult oxidation reactions are catalyzed by diiron enzymes and as a result there is a lot of interest in generating synthetic analogues for the production of fine chemicals. These synthetic analogues allow one to study the active site region of these enzymes without perturbations of the protein environment.[9,10] Synthetic biomimetic models of MMO and RNR have been amply studied.[9] For instance, the biomimetic complex $[Fe_2(6\text{-HPA})(\mu\text{-O})(H_2O)_2]^{4+}$ (6-HPA = 1,2-bis[2-{bis(2-pyridylmethyl)aminomethyl}-6-pyridyl]ethane) reacts with alkenes to generate epoxides efficiently.[11] More recent studies by Suzuki et al on peroxodiiron complexes with a bridging carboxylate ligand gave different reactivity patterns for a bridging Ph_3CCOO^- versus Ph_3COO^- group.[12] In particular, the system with Ph_3COO^- ligand gave regioselective phenyl hydroxylation, whereas the one with Ph_3CCOO^- ligand exhibited reversible deoxygenation. Therefore, seemingly small perturbations to the ligand system bound to the diiron core can influence the inherent and catalytic properties of the system. Crystal structures and spectroscopic properties of synthetic (μ-hydroxo)-(μ-peroxo)diiron and (μ-oxo)(μ-peroxo)diiron complexes with a tripodal ligand (6-Me_2-BPP = *N*,*N*-bis(6-methyl-2-pyridylmethyl)-3-aminopropionate) were studied and the system shows spectroscopic properties and vibrational $^{16}O_2/^{18}O_2$ isotope shifts at par with carboxylate-bridged diiron enzyme complexes as appear in RNR, Δ^9D, and ferritin.[13] In this work we will describe the electronic and catalytic properties of (μ-oxo)(μ-peroxo)diiron-BPP_2 complex versus a typical substrate and make predictions of reactivities of analogous complexes in the RNR active site.

Extensive studies on diiron biomimetics have been performed and crystal structures and spectroscopic parameters of key intermediates after dioxygen activation determined.[14] Thus, spectroscopic studies revealed that an initial μ-hydroxodiiron(II) complex reacts with molecular oxygen to form an end-on dioxygen-μ-hydroxodiiron(II,III) complex, which, via a proton-coupled electron transfer, is converted into $HOO(Fe^{III})(O)(Fe^{III})(OH)$.[15] The latter structure looses water to generate a μ-oxo-μ-1,2-peroxo complex. Despite extensive studies on this and similar systems, it is unknown which of these complexes is the actual active oxidant in the catalysis of substrates. Recent studies on toluene monoxygenase implicated that a peroxo-bridged diiron complex could act as the active species of this enzyme.[16] However, these studies contradict work on mononuclear iron complexes for which the hydroperoxoiron species was shown to be a sluggish oxidant toward epoxidation especially in comparison to the oxoiron system.[17] Therefore, to shed light onto the mechanism by which diiron complexes react with substrates we present here density functional theory studies on the propene epoxidation by a μ-oxo-μ-peroxodiiron complex and try to elucidate whether this complex can act as the active oxidant of substrates.

Synthetic complexes with oxo-bridged diiron units have been known for quite some time for systems with porphyrin ligands.[18] Recently, it was shown that nonheme oxoiron(IV) complexes exchange the oxygen atom with other nonheme iron complexes rapidly, at a rate proportional to the oxidizing power of the oxoiron(IV) catalyst.[18d] Karlin et al[19] studied oxo, hydroxo, and peroxo dimetal complexes using iron, cobalt, and copper mixtures with one metal atom located in a porphyrinate ligand, and the other in a tris(2-pyridylmethyl)amine ligand. Crystal structures of μ-oxodiiron and μ-oxocopper iron complexes were measured.

The earliest density functional theory studies of a peroxo-bridged diiron biomimetic were carried out by Brunold and Solomon et al.[20] These studies addressed the spectroscopic properties of a μ-peroxodi-μ-carboxylate diiron complex. The ligands bound to the metal were abbreviated with ammonia molecules, and the carboxylic acid residues with formic acid. Only the maximum spin structure with $S = 5$ was calculated, but the results in general were in good agreement with experimental work. Further computational studies of diiron enzyme models have been reported for ferritin, MMO, and RNR.[21–23] Essentially, the active site structures of RNR and MMO are quite similar and the diiron center is bound to five carboxylic acid groups of aspartate or glutamate amino acids and two imidazole groups of histidine residues. Furthermore, dependent on the oxidation state of the system, the remaining ligand sites on the iron atoms are occupied by water molecules, a μ-oxo group, or a hydroxo group. It was concluded that the O–O bond cleavage of dioxygen in MMO and RNR enzymes differs due to a nearby tryptophan radical in RNR that facilitates a fast electron transfer process and lowers the O–O bond-breaking barrier.[22d] A ferritin mimic containing a μ-oxo-μ-peroxodiiron core was shown to be stable in a protein environment.[21] Detailed studies on the reaction mechanism of methane hydroxylation by MMO were done by Yoshizawa and Yumura.[24] Possible reaction pathways were investigated as well as detailed vibrational analysis of possible intermediates in the reaction process.

In the past we extensively studied oxoiron heme and nonheme complexes and their reactivity patterns with respect to typical substrates.[25] It was shown that generally nonheme oxoiron systems are stronger and more potent catalysts than heme-type oxoiron complexes.[25b,26] To find out whether the catalytic properties of diiron systems match ones of mononuclear iron complexes or what their fundamental differences are we have performed DFT calculations on $[Fe_2(BPP)_2(O)(O_2)]$ with BPP = *N*,*N*-bis(2-pyridylmethyl)-3-ami-

nopropionate), see Scheme 1. BPP is a tetradentate ligand that binds to iron through its two pyridine nitrogen atoms, the amino nitrogen atom, and one of the oxygen atoms of

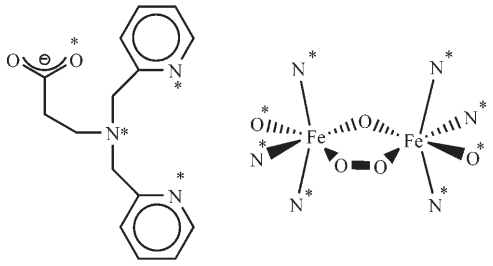

Scheme 1. Chemical structure of the BPP ligand studied in this work. The atoms labeled with a star bind to iron.

the carboxylate group (atoms labeled with a star in Scheme 1). Although many experimental biomimetic studies have been performed on similar complexes, their electronic and catalytic properties are still shrouded in many mysteries. Moreover, understanding the mechanisms of substrate oxidation by typical diiron complexes will explain the nature of diiron enzymes. Therefore, to gain insight into the reaction of diiron complexes with oxygen and the possible subsequent monoxygenation of a substrate, we present here results of the density functional theory study into the properties of $[Fe_2(BPP)_2(O)(O_2)]$ and its monoxygenation of a typical substrate (propene). We will compare the results with those of previous studies of diiron enzyme models and mononuclear oxoiron catalysts.[22–25,27]

Results and Discussion

Electronic properties of $[Fe_2O_3(BPP)_2]$: Diiron centers are known to possess an extensive set of unpaired electrons on both iron atoms.[20–24] Indeed, also the μ-oxo-μ-peroxodiiron $(BPP)_2$ complex (**1**) has many close-lying electronic states with different possible orbital occupations. Figure 2 shows a schematic representation of the highest lying occupied and low-lying virtual orbitals of **1**. The orbitals are dominated by the 3d atomic orbitals on the two iron centers, which split into a typical t_{2g}–e_g type of system with three low-lying π* orbitals (π^*_{xy}, π^*_{FeO}, and π^*_{FeOO}) and two high-lying σ* orbitals ($\sigma^*_{x^2-y^2}$ and $\sigma^*_{z^2}$) (Figure 2a). The π^*_{xy} orbital is essentially a nonbonding orbital on the metal in the plane of the Fe_2O_3 ring (the *xy* plane), while the π^*_{FeO} and π^*_{FeOO} orbitals represent the interactions of the $3d_{xz,yz}$ atomic orbitals on iron with the $2p_{x,y}$ atomic orbitals on the oxo group and the peroxo group, respectively. The two σ* orbitals reflect the antibonding interactions of the metal with the ligands in the plane of the Fe_2O_3 ring ($\sigma^*_{x^2-y^2}$) or perpendicular to this plane ($\sigma^*_{z^2}$). Both metal centers have $3d^5$ occupation in all

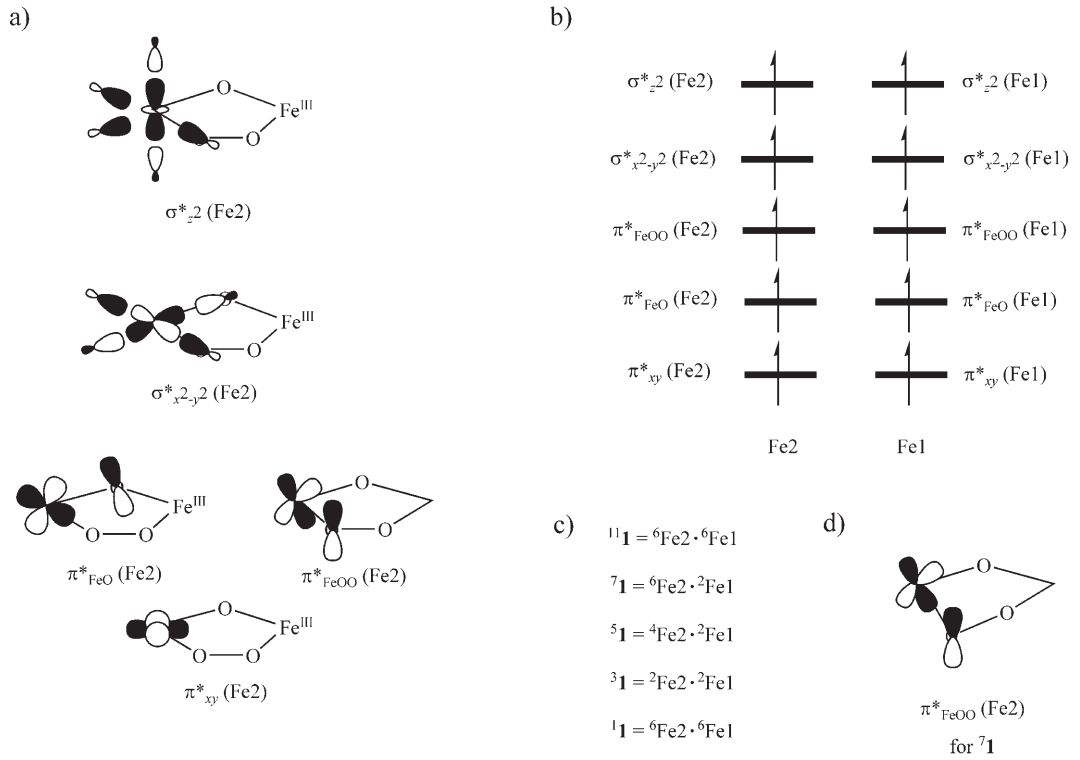

Figure 2. a) Metal 3d block molecular orbitals of **1** with coefficients on metal Fe2. There is a similar set of orbitals on Fe1 (not shown). b) Orbital occupation of ^{11}**1**; orbitals on the left are on Fe2 and the ones on the right on Fe1. c) Local spin character on each metal atom for ^{11,7,5,3,1}**1**. d) Distorted π^*_{FeOO} orbital as observed in ^{7}**1**.

structures and hence the metals are in the oxidation state Fe^{III} in all spin states. To test the relative energies of the possible spin-state structures we calculated **1** in the singlet, triplet, quintet, septet, and undecaplet spin states. The undecaplet and open-shell singlet structures have the two metal 3d blocks completely singly occupied, and the five unpaired electrons on each iron center are ferromagnetically or antiferromagnetically coupled (Figure 2b). Thus, ^{11}**1** and ^{1}**1** essentially can be seen as two neighboring sextet iron atoms: ^{6}Fe1·^{6}Fe2 (Figure 2c). By contrast, the septet spin state in fact has a sextet spin orientation on Fe2 ferromagnetically coupled to a doublet spin on Fe1 with orbital occupation $\pi^*_{xy}{}^2\ \pi^*_{FeO}{}^2\ \pi^*_{FeOO}{}^1$. In the quintet spin state, there is also a doublet spin on Fe1, but it is ferromagnetically coupled to a quartet spin on Fe2 with $\pi^*_{xy}{}^2\ \pi^*_{FeO}{}^1\ \pi^*_{FeOO}{}^1\ \sigma^*_{z^2}{}^1$ occupation. Finally, the triplet spin state structure represents the ferromagnetically coupled system with a doublet spin on each metal atom, whereby one center has $\pi^*_{xy}{}^2\ \pi^*_{FeO}{}^2\ \pi^*_{FeOO}{}^1$ occupation, whereas the other $\pi^*_{xy}{}^2\ \pi^*_{FeO}{}^1\ \pi^*_{FeOO}{}^2$ occupation so that the two radicals are on opposite sides of the Fe_2O_3 ring.

We ran a full geometry optimization of the (μ-oxo)(μ-1,2-peroxo)$(BPP)_2$diiron complex (**1**) in the singlet, triplet, quintet, septet, and undecaplet spin states. The open-shell singlet state is the ground state and is 5.8 kcal mol^{-1} lower in energy than the undecaplet spin state. The other spin-state structures are considerably higher in energy: ^{7}**1** is 17.3 kcal mol^{-1} above ^{1}**1**, whereas the quintet and triplet spin states are 30.0 and 40.1 kcal mol^{-1} higher, respectively. Therefore, we will focus the remaining discussion on the broken spin singlet and undecaplet spin states only; all other results can be found in the Supporting Information. Since, ^{1}**1** and ^{11}**1** are close in energy, it is expected that **1** will react via two-state reactivity (TSR) patterns on competing singlet and undecaplet spin-state surfaces. TSR has been shown to be very dominant for heme-type oxoiron systems, such as the active species of cytochrome P450 enzymes.[25a,28] The oxoiron species of P450 has close-lying doublet and quartet spin states with the same orbital occupation that are separated by less than 1 kcal mol^{-1}. However, the electron transfer mechanisms and reaction mechanisms differ sometimes on the two spin state surfaces so that for example, on one spin state surface rearranged products are formed, whereas on the other one only unrearranged products are observed.[29]

Optimized geometries of ^{1}**1** and ^{11}**1** are shown in Figure 3. Owing to the same orbital occupation of these two spin states their optimized geometries are very similar. Most bond lengths in ^{1,11}**1** are within 0.01 Å, except the Fe1–O3 and Fe2–O5 distances that differ by 0.084 and 0.056 Å, respectively. As a result of that the Fe1-O4-O5-Fe2 dihedral angle is closer to planarity in ^{1}**1**. Geometrically, the iron–ligand distances show some fluctuations between the various spin states due to differences in charge and spin populations on the two iron centers. For instance, the π^*_{FeO} orbital on Fe1 is singly occupied in ^{11}**1**, but doubly occupied in other spin states; as a result a much longer Fe–O distance is obtained in ^{11}**1** than in ^{3,5,7}**1**. Furthermore, single occupation of

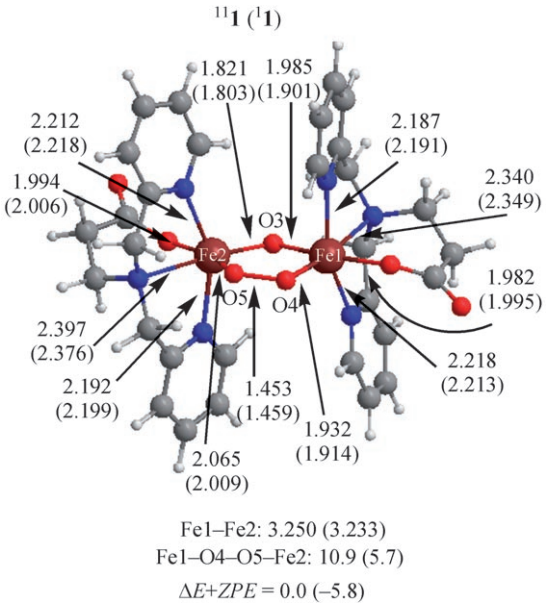

Figure 3. Optimized UB3LYP/B1 geometries of ^{11,1}**1** with iron–ligand distances (in Å). Also shown are the relative energies (in kcal mol^{-1}) with respect to ^{11}**1**, the dihedral angle Fe1-O4-O5-Fe2 (in deg) and the interatomic iron–iron distance.

the two σ* orbitals in ^{7}**1** leads to enhanced distances between Fe2 and its ligands due to more antibonding character into these bonds, whereas the corresponding bonds on Fe1 are much shorter. Therefore, the geometric features of the different spin state structures follow the orbital occupation of Figure 2.

The peroxo moiety is considerably displaced from the μ-oxodiiron plane in the septet and quintet spin states by more than 45°, whereas it is almost in the plane (by 5.7°, 8.7°, and 10.9°, respectively) in the singlet, triplet, and undecaplet spin states. The large dihedral angle in the septet and quintet spin states is the result of a doublet spin state on one iron center with $\pi^*_{xy}{}^2\ \pi^*_{FeO}{}^2\ \pi^*_{FeOO}{}^1$ occupation, which shortens one Fe–O bond. At the same time the Fe–OO bond opposite in the Fe_2O_3 ring is weakened and the oxygen atom of the peroxo group is displaced from the oxodiiron plane. As a consequence, this changes the π^*_{FeOO} orbital on the sextet spin iron center (Figure 2d) considerably and provides bonding overlap between the $2p_y$ atomic orbital on oxygen with the $3d_{yz}$ orbital on Fe1 rather than antibonding character. Therefore, the ring will be close to planarity in situations for which the two metal atoms are electronically identical, that is, with similar orbital occupation on both metal centers as is the case in ^{11}**1**, ^{1}**1**, and ^{3}**1**, that is, ^{11}**1** and ^{1}**1** contain two (anti)ferromagnetically coupled sextet iron atoms, whereas in ^{3}**1** two doublet spin iron atoms are coupled (Figure 2c). Thus, double occupation of the π^*_{FeO} orbital on one center and single occupation on the other metal center changes the spin and charge polarization in the peroxo group, resulting in tilting of the peroxo group out of the oxodiiron plane. Experimentally, also a small FeOOFe dihedral angle of 14.5° is observed for a μ-hydroxo-μ-1,2-

peroxodiiron complex,[13] which is close to the one we obtain here for ^{1,11}**1**. Even though this dihedral angle shows considerable differences between the various calculated structures, the interatomic Fe–Fe distance is virtually the same in all spin states (3.151–3.244 Å). Generally, the optimized geometries compare well with those from the crystal structure determined by Suzuki et al.[13]

Vibrational spectra and isotopic replacement of the peroxo group: It has been shown that peroxodiiron complexes have a vibrational spectrum that undergoes some significant changes when one (or both) of the atoms of the peroxo group are replaced by a heavier isotope (Table 1).[2–5] Thus, the O–O stretch vibrations are located at 870 cm^{-1} in RNR, at 898 cm^{-1} in Δ^9D, and at 851 cm^{-1} in ferritin, but replacement of the $^{16}O_2$ peroxo group with $^{18}O_2$ lowers these stretch vibrations by a value $\delta = 46$–53 cm^{-1} (Table 1).[2,3,5a] Synthetic biomimetic complexes with a μ-peroxodiiron core give a peroxo stretch vibration (ν_{OO}) and subsequent $^{18}O_2$ isotopic change (δ) of the same order of magnitude as the enzymatic systems.[12,13,15] The symmetrical ($\nu_{s,OFeOO}$) and asymmetrical ($\nu_{as,OFeOO}$) stretch vibrations in the Fe-O-O-Fe groups of the enzymes are typically located between 442–485 cm^{-1} and between 490–500 cm^{-1}, respectively. These two vibrations also show sensitivity to isotopic substitution, but by a much smaller degree than the O–O stretch vibration, that is, both vibrations drop by 12–22 cm^{-1} after replacement of the $^{16}O_2$ peroxo group by $^{18}O_2$.

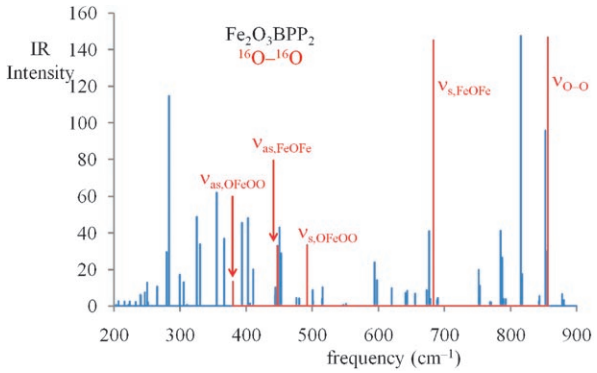

Figure 4. a) Vibrational spectrum of $^1Fe_2(BPP)_2(O)(O_2)$ in the range of 200–900 cm^{-1}. Highlighted are critical vibrations for the Fe_2O_3 core.

Table 1. Selected vibrational frequencies (ν) of peroxodiiron complexes and the change of the frequency (δ) after substitution of $^{16}O_2$ by $^{18}O_2$.[a,b]

System	ν_{OO}	δ	$\nu_{s,OFeOO}$	δ	$\nu_{as,OFeOO}$	δ	Ref.
enzymes:							
RNR	870	−46	458	−16	499	−22	[2]
Δ^9D	898	−53	442	−17	490	−19	[5a]
ferritin	858	−51	485	−17	499	−12	[3]
synthetic models:							
$[Fe_2(6\text{-}Me_2\text{-}BPP)_2(O)(O_2)]$	847	−33	465	−19	570	−28	[13]
$[Fe_2(6\text{-}Me_3\text{-}TPA)_2(O)(O_2)]^{2+}$	848	−46	462	−21	531	−21	[15]
$[Fe_2(LPh_4)(Ph_3CCOO)(O_2)]^{2+}$	873	−50	480	−16			[12]
$[Fe_2(LPh_4)(PhCOO)(O_2)]^{2+}$	840	−45	459	−20			[12]
calculations:							
$^1Fe_2(BPP)_2(O)(O_2)$	856	−48	380	−15	492	−19	[c]
$^{11}Fe_2(BPP_2)(O)(O_2)$	848	−48	434	−8	580	−19	[c]

[a] Vibrational frequencies (in cm^{-1}) obtained at UB3LYP/LACVP. [b] δ is frequency shift in cm^{-1} for $^{16}O_2$-peroxide replaced by $^{18}O_2$ peroxide. [c] This work.

We have calculated the vibrational frequencies of ^{1}**1** and ^{11}**1** and highlights of the results are shown in Figure 4 and Table 1. Our calculated ν_{OO} of 856 and 848 cm^{-1} for ^{1}**1** and ^{11}**1**, respectively, is in perfect agreement with the experimental value for $[Fe_2(6\text{-}Me_2\text{-}BPP)_2(O)(O_2)]$ obtained by Suzuki et al.[13] and shows a similar sensitivity to $^{18}O_2$ substitution. A comparable value for ν_{OO} was obtained in the septet spin state, which implies that the O–O stretch vibration is not sensitive to the Fe-O-O-Fe dihedral angle in the geometry. The value also matches the O–O stretch vibration in other synthetic μ-peroxodiiron complexes and ferritin closely (Table 1).[3,12,13,15] The symmetrical stretch vibration ($\nu_{s,OFeOO}$) is close to the one observed for synthetic biomimetics and enzymes especially for ^{11}**1**, but the effect of ^{18}O substitution is here much smaller. Finally, the asymmetrical stretch vibration in ^{1}**1** ($\nu_{as,OFeOO}$) as calculated is close to the one observed for enzymatic systems but considerably lower lying than the one in typical peroxodiiron enzyme systems. On the other hand, the $\nu_{as,OFeOO}$ value of ^{11}**1** is close to that for the synthetic model developed by Suzuki et al.[13] and quite different from enzymatic systems. It may be anticipated that these $\nu_{as,OFeOO}$ values indicate that enzymatic systems are low-spin and biomimetic complexes are high-spin but this needs to be tested in further studies. The symmetrical ($\nu_{s,FeOFe}$) and asymmetrical ($\nu_{as,FeOFe}$) stretch vibrations for the μ-oxodiiron group are located at 447 and 683 cm^{-1}, respectively, for ^{1}**1** and at 420 and 640 cm^{-1} for ^{11}**1**. The differences between ^{1}**1** and ^{11}**1** for the symmetrical and asymmetrical oxoiron stretch vibrations are due to the geometric differences of ^{1}**1** and ^{11}**1** (Figure 3). Needless to say, only minor changes are observed in these oxoiron vibrations after isotopic substitution of the peroxo group with $^{18}O_2$.

Catalytic properties of $[Fe_2O_3(BPP)_2]$: Experimental studies on RNR and MMO enzymes failed to elucidate the active catalyst that performs the monoxygenation reaction.[30] Thus, it has been anticipated that the peroxo-bridged diiron(III) complex in MMO is able to perform alkene epoxidation, whereas a μ-dioxodiiron complex might hydroxylate alkanes. To establish whether a (μ-oxo)(μ-1,2-peroxo)diiron complex similar in structure to **1** is able to epoxidize C=C double bonds, we have calculated the epoxidation mechanism of

propene by **1**. As shown in Figure 3 the broken spin singlet spin state is the ground state with the undecaplet spin state a few kcal mol^{-1} higher. These two spin states are well separated from the other spin states. Detailed geometry scans starting from ^{1,11}**1** for the C–O bond formation reaction between the peroxo group and the approaching propene molecule led to a high-energy epoxidation pathway (with barriers in excess of 35 kcal mol^{-1}) (Figure 5). During these scans the

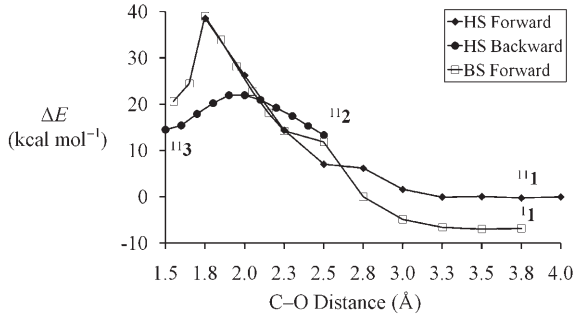

Figure 5. a) Forward and backward geometry scans for the C–O activation reaction. Each point corresponds to a full geometry optimization with one degree of freedom (the C–O distance) fixed. All energies are in kcal mol^{-1} relative to ^{11}**1** and are obtained at UB3LYP/B1 in Jaguar. The forward scan started from ^{11,1}**1**, while the backward scan started from ^{11}**2**. b) Reaction mechanisms of propene epoxidation via a direct pathway or via the μ-oxo-μ-1,1,-peroxodiiron intermediate (**2**).

Fe_2O_3 ring stayed virtually intact right up until the C–O bond formation, whereby a radical on the substrate moiety was created. We then removed the geometric constraints and did a full optimization of the epoxide radical intermediate (**3**), whereby the terminal oxygen atom of the peroxide moiety forms a bond with propene and a radical center is created on the substrate. Thus, a backward geometry scan starting from the epoxide intermediate (^{11}**3**) in the direction of **1**, showed that much lower barriers are encountered but led to a side-on peroxodiiron complex or (μ-oxo)(μ-1,1-peroxo) [Fe_2O_3(BPP)$_2$] complex (^{11}**2**) rather than ^{11}**1**. Thus, the exploratory geometry scans implicated that the (μ-oxo)(μ-1,2-peroxo)diiron complex (**1**) first is converted into a (μ-oxo)(μ-1,1-peroxo) diiron complex (**2**) that is able to react with substrates with much lower reaction barriers than a direct epoxidation by **1**. Therefore, we started the work with studies of the ring-opening of the Fe_2O_3 cluster in the singlet, septet, and undecaplet spin states to form complex ^{1,7,11}**2**.

Detailed geometry scans for the conversion of **1** into **2** are shown in Figure 6. Thus the conversion of ^{11}**1** (^{1}**1**) into ^{11}**2** (^{1}**2**) encounters a barrier of 7.9 (8.8) kcal mol^{-1} and is endothermic by 5.7 (2.9) kcal mol^{-1}. Indeed, this barrier is significantly lower than that for the direct epoxidation mechanism, as shown in Figure 5. Therefore, it may very well be that an internal reorganization, that is, conversion of **1** into **2** precedes the catalytic mechanism.

Subsequently, we calculated the epoxidation of propene by ^{11,7,5,3,1}**2**, and the potential energy surface obtained is

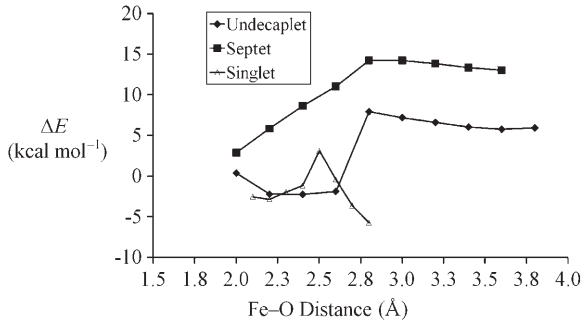

Figure 6. Geometry scan for the conversion of the μ-oxo-μ-1,2-peroxo (^{11,7,1}**1**) into the μ-oxo-μ-1,1-peroxo (**2**) complex. Each point corresponds to a full geometry optimization with one degree of freedom (the Fe–O distance) fixed. All energies are in kcal mol^{-1} relative to ^{11}**1** and are obtained at the UB3LYP/B1 level of theory in Jaguar.

shown in Figure 7, including optimized geometries of the radical intermediate (^{1,11}**3**) and epoxide product complexes (^{1,11}**4**). Optimized geometries of all structures are given in the Supporting Information. Thus, the reactions occur in stepwise fashion via an initial C–O bond formation transition state (**TS1**), which leads to a radical intermediate (**3**) that via a ring-closure transition state (**TS2**) gives epoxide products and a di-μ-oxodiiron complex (**4**). All energies reported are $\Delta E + ZPE$ values with energies obtained with B2 and ZPE corrections with B1 basis sets and calculated relative to ^{11}**1**. The mechanism is similar to ones calculated for mononuclear heme and nonheme catalysts.[25–27] Note that the ring-closure barriers (**TS2**) are of the same order of magnitude as the C–O bond formation barriers (**TS1**) on all four spin states, which implies that the reaction will be of second order kinetics with a relatively long-lived radical intermediate (**3**). During the lifetime of this intermediate rearrangement may occur leading to *cis–trans* scrambling of epoxides as shown before for the epoxidation of ethene and styrene by P450 model complexes.[31] Although the exothermicity of the overall reaction is large (36.4 kcal mol^{-1} for the undecaplet spin state), the reaction encounters a large C–O bond formation barrier. The lowest barrier is via ^{1}**TS1** with the barrier via ^{11}**TS1** some 2.5 kcal mol^{-1} higher. Thus, the μ-oxo-peroxodiiron complex reacts via two-state reactivity on competing singlet and undecaplet spin state surfaces. However, the absolute barriers are significant, with ^{1}**TS1** being 29.4 kcal mol^{-1} above ^{11}**1**. These barriers are too high to be considered as a realistic oxidant of epoxidation reactions. The barriers passing ^{7}**TS1**, ^{5}**TS1**, and ^{3}**TS1** are higher in energy than ^{11}**TS1** by 11.8, 27.1, and 25.6 kcal mol^{-1}. Thus, with rate-determining epoxidation barriers of the order of 30 kcal mol^{-1} or more, it is not expected that the μ-oxo-μ-peroxo (BPP)$_2$ diiron complex will be an efficient catalyst of epoxidation reactions. In particular, with the same methods and basis sets the epoxidation of propene by a cytochrome P450 mimic gave barriers of 12.3 kcal mol^{-1}, whereas a nonheme mimic of taurine/α-ketoglutarate dioxygenase gave a barrier of 4.8 kcal mol^{-1}.[25b,32] Therefore, the (μ-oxo)(μ-1,1-

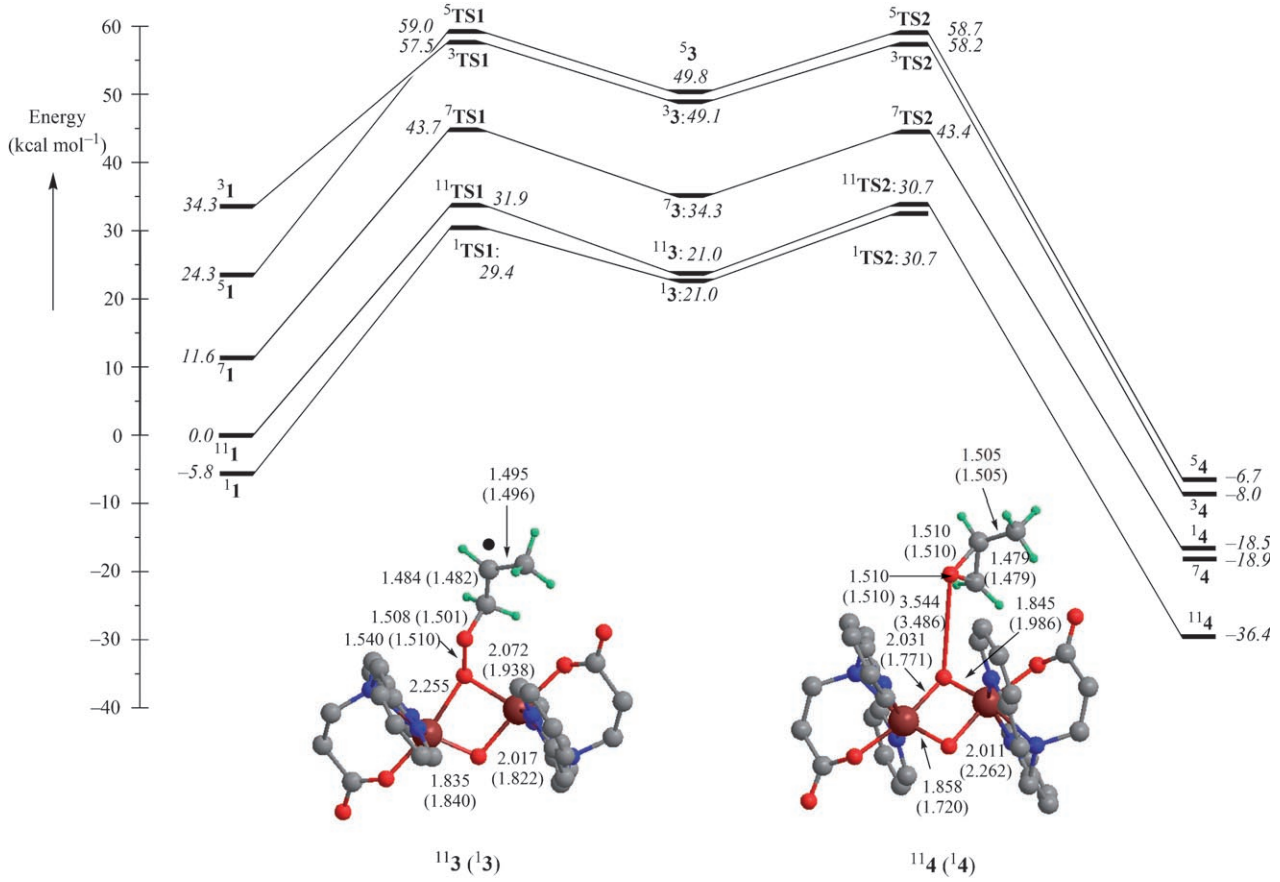

Figure 7. Potential energy landscape for the epoxidation of propene by ^{11,7,5,3,1}**2**. All energies are in kcal mol^{-1} relative to ^{11}**1** and have been taken from the $\Delta E + ZPE$ values with energies at the UB3LYP/B2 level of theory and ZPE corrections at the UB3LYP/B1 level of theory.

peroxo) and (μ-oxo)(μ-1,2-peroxo)diiron complexes are sluggish oxidants that are unable to react with substrates.

As such, another intermediate in the catalytic cycle of RNR and related biomimetics is responsible for substrate hydroxylation and/or epoxidation. Nevertheless, the complete reaction mechanism leading to epoxide products is still exothermic by a large amount, so that there should be a mechanism with lower barriers for this diiron system. The catalytic cycle of this biomimetic contains many intermediates that could be alternative oxidants in this process. Moreover, it may very well be that the peroxodiiron species abstracts a proton from its surrounding to create the active oxidant. Therefore, many possible oxidants in this catalytic mechanism remain and the search to identify this elusive oxidant continues. Work is in progress in our group to establish the active oxidant in this reaction.

Thus, our calculations show that neither the μ-oxo-μ-1,2-peroxodiiron complex nor the μ-oxo-μ-1,1-peroxodiiron complex is likely to act as the active oxidant in hydroxylation or epoxidation reactions of substrates. As a consequence of this, it is also unlikely that precursors of the μ-oxo-μ-1,2-peroxodiiron complex in the catalytic cycle of this system are active oxidants as that would prevent the occurrence of the μ-oxo-μ-peroxodiiron complex. Therefore, it seems more likely that the μ-oxo-μ-1,2-peroxodiiron complex is an intermediate en route to the formation of the active oxidant of RNR and biomimetics rather than the actual catalyst itself. Thus, it may very well be that the active oxidant is so reactive that it cannot be stabilized and detected and that the μ-oxo-μ-1,2-peroxodiiron complex is the last intermediate in the catalytic cycle which is inactive and can be stabilized long enough to be detected and characterized. This is, for instance, the case in the cytochromes P450 for which the active oxidant is elusive and has never been detected experimentally. However, indirect evidence of the nature of the active oxidant was obtained through kinetic isotope effect studies and product distributions that implicated the oxoiron species as the active oxidant in P450 catalysis, although controversies regarding possible alternative oxidants remain.[25a,33]

Conclusion

DFT calculations on a synthetic diiron model mimicking the active site of diiron enzymes such as RNR, ferritin, and Δ^9D have been performed. The calculations predict electronic, spectroscopic and structural features of the μ-oxo-μ-peroxodiiron complex. Thus, vibrational spectra are in excellent agreement with experiment and the replacement of $^{16}O_2$ by

$^{18}O_2$ in the peroxo moiety gives a spectroscopic downshift of the peroxo O–O stretch vibration with $-48\ cm^{-1}$ when both oxygen atoms are substituted by ^{18}O atoms. Subsequent, reactivity studies of the μ-oxo-μ-1,2-peroxo species revealed that it is a sluggish oxidant with high epoxidation barriers with respect to propene. We then investigated an alternative mechanism in which the μ-oxo-μ-1,2-peroxo is converted into a μ-oxo-μ-1,1-peroxo species. This structural rearrangement is a low-energy pathway that is slightly endothermic. The epoxidation reaction from the μ-oxo-μ-1,1-peroxo species gave substantially lower epoxidation barriers than the pathway from the μ-oxo-μ-1,2-peroxo intermediate but the barriers are still considerably higher than those obtained for mononuclear heme and nonheme oxoiron catalysts. Therefore, the μ-oxo-μ-peroxodiiron intermediate in biomimetics and enzymatic systems cannot be regarded as an active oxidant of epoxidation reactions. Research continues to search for the catalytic active species in RNR enzymes.

Experimental Section

As before[25,26] all calculations employ the unrestricted hybrid density functional method UB3LYP,[34] since this method has been shown to produce rate constants and kinetic isotope effects at par with experimental data.[29,35] We used (μ-oxo)(μ-peroxo)$(BPP)_2$diiron ($Fe_2C_{30}H_{32}N_6O_7$) as catalyst, and propene as substrate. Full geometry optimizations (without constraints) were performed in Jaguar, but since Jaguar does not have the possibility to calculate frequencies analytically these were done with Gaussian-03.[36,37] Previous work of ours has shown that a numerical frequency in Jaguar gives energetics and frequencies similar to an analytical frequency in Gaussian.[37] All transition states reported here had one imaginary frequency for the correct mode, while all reactants, products, and intermediates had real frequencies only. Initially we used a double-ζ type LACVP basis set on iron (that contains a core potential) and a 6-31G basis set on the rest of the atoms: basis set B1.[38] Subsequent single-point calculations on the optimized geometries using the triple-ζ type LACV3P+ basis set on iron and 6-311+G* on all other atoms were performed in Jaguar: basis set B2. All energies reported in this work were taken from the UB3LYP/B2 energies with zero-point corrections at the UB3LYP/B1 level of theory. As is the case in most transition-metal complexes,[39] the reactants appear in close-lying spin states; therefore, we calculated the complete reaction pathway on the singlet, triplet, quintet, septet, and undecaplet spin states, which are identified with a superscript 1, 3, 5, 7, and 11 next to the label of the structure. In this work we focused on the lowest lying two spin states, namely the maximum spin state and its antiferromagnetic counterpart with an overall spin of $S=0$. All data on the remaining spin states can be found in the Supporting Information. We ran extensive geometry scans between reactants, intermediates, and product complexes. These calculations were performed with Jaguar and correspond to a full geometry optimization with one degree of freedom fixed, that is, the reaction coordinate. These calculations were used to confirm the reaction mechanisms between the various local minima and to create starting points for the transition-state optimizations.

Acknowledgements

The National Service of Computational Chemistry Software (NSCCS) is acknowledged from providing CPU time. Prof. Lawrence Que, Jr. is acknowledged for fruitful discussions on the work.

[1] E. Y. Tshuva, S. J. Lippard, *Chem. Rev.* **2004**, *104*, 987–1012.
[2] a) P. Moënne-Loccoz, J. Baldwin, B. A. Ley, T. M. Loehr, J. M. Bollinger, Jr., *Biochemistry* **1998**, *37*, 14659–14663; b) D. Yun, R. García-Serres, B. M. Chicalese, Y. H. An, B. H. Huynh, J. M. Bollinger, Jr., *Biochemistry* **2007**, *46*, 1925–1932.
[3] P. Moënne-Loccoz, C. Krebs, K. Herlihy, D. E. Edmondson, E. C. Theil, B. H. Huynh, T. M. Loehr, *Biochemistry* **1999**, *38*, 5290–5295.
[4] A. M. Valentine, S. S. Stahl, S. J. Lippard, *J. Am. Chem. Soc.* **1999**, *121*, 3876–3887.
[5] a) J. A. Broadwater, J. Ai, T. M. Loehr, J. Sanders-Loehr, B. G. Fox, *Biochemistry* **1998**, *37*, 14664–14671; b) B. G. Fox, K. S. Lyle, C. E. Rogge, *Acc. Chem. Res.* **2004**, *37*, 421–429.
[6] K. R. Strand, S. Karlsen, M. Kolberg, Å. K. Røhr, C. H. Görbitz, K. K. Andersson, *J. Biol. Chem.* **2004**, *279*, 46794–46801.
[7] G. D. Straganz, B. Nidetzky, *ChemBioChem* **2006**, *7*, 1536–1548.
[8] a) J. R. O'Brien, D. J. Schuller, V. S. Yang, B. D. Dillard, W. N. Lanzilotta, *Biochemistry* **2003**, *42*, 5547–5554; b) P. J. Riggs-Gelasco, J. C. Price, R. B. Guyer, J. H. Brehm, E. W. Barr, J. M. Bollinger, Jr., C. Krebs, *J. Am. Chem. Soc.* **2004**, *126*, 8108–8109; c) J. M. Bollinger, Jr., J. C. Price, L. M. Hoffart, E. W. Barr, C. Krebs, *Eur. J. Inorg. Chem.* **2005**, 4245–4254.
[9] a) E. I. Solomon, T. C. Brunold, M. I. Davis, J. N. Kemsley, S.-K. Lee, N. Lehnert, F. Neese, A. J. Skulan, Y.-S. Yang, J. Zhou, *Chem. Rev.* **2000**, *100*, 235–349; b) M. Costas, M. P. Mehn, M. P. Jensen, L. Que, Jr., *Chem. Rev.* **2004**, *104*, 939–986.
[10] a) M. J. Ryle, R. P. Hausinger, *Curr. Opin. Chem. Biol.* **2002**, *6*, 193–201; b) S. V. Kryatov, E. V. Rybak-Akimova, S. Schindler, *Chem. Rev.* **2005**, *105*, 2175–2226.
[11] M. Kodera, M. Itoh, K. Kano, T. Funabiki, M. Reglier, *Angew. Chem.* **2005**, *117*, 7266–7268; *Angew. Chem. Int. Ed.* **2005**, *44*, 7104–7106.
[12] M. Yameshita, H. Furutachi, T. Tosha, S. Fujinami, W. Saito, Y. Maeda, K. Takahashi, K. Tanaka, T. Kitagawa, M. Suzuki, *J. Am. Chem. Soc.* **2007**, *129*, 2–3.
[13] X. Zhang, H. Furutachi, S. Fujinami, S. Nagatomo, Y. Maeda, Y. Watanabe, T. Kitagawa, M. Suzuki, *J. Am. Chem. Soc.* **2005**, *127*, 826–827.
[14] a) Y. Dong, Y. Zang, L. Shu, E. C. Wilkinson, L. Que, Jr., K. Kauffmann, E. Münck, *J. Am. Chem. Soc.* **1997**, *119*, 12683–12684; b) H. Zheng, S. J. Yoo, E. Münck, L. Que, Jr., *J. Am. Chem. Soc.* **2000**, *122*, 3789–3790; c) S. V. Kryatov, E. V. Rybak-Akimova, V. L. MacMurdo, L. Que, Jr., *Inorg. Chem.* **2001**, *40*, 2220–2228; d) M. Costas, C. W. Cady, S. V. Kryatov, M. Ray, M. J. Ryan, E. V. Rybak-Akimova, L. Que, Jr., *Inorg. Chem.* **2003**, *42*, 7519–7530; e) S. V. Kryatov, F. A. Chavez, A. M. Reynolds, E. V. Rybak-Akimova, L. Que, Jr., W. B. Tolman, *Inorg. Chem.* **2004**, *43*, 2141–2150; f) S. V. Kryatov, S. Taktak, I. V. Korendovych, E. V. Rybak-Akimova, J. Kaizer, S. Torelli, X. Shan, S. Mandal, V. L. MacMurdo, A. Mairata i Payeras, L. Que, Jr., *Inorg. Chem.* **2005**, *44*, 85–99.
[15] a) V. L. MacMurdo, H. Zheng, L. Que, Jr., *Inorg. Chem.* **2000**, *39*, 2254–2255; b) X. Shan, L. Que, Jr., *Proc. Natl. Acad. Sci. USA* **2005**, *102*, 5340–5345.
[16] L. J. Murray, S. G. Naik, D. O. Ortillo, R. García-Serres, J. K. Lee, B. H. Huynh, S. J. Lippard, *J. Am. Chem. Soc.* **2007**, *129*, 14500–14510.
[17] a) M. J. Park, J. Lee, Y. Suh, J. Kim, W. Nam, *J. Am. Chem. Soc.* **2006**, *128*, 2630–2634; b) W. Nam, *Acc. Chem. Res.* **2007**, *40*, 522–531.
[18] a) D.-H. Chin, G. N. La Mar, A. L. Balch, *J. Am. Chem. Soc.* **1980**, *102*, 5945–5947; b) A. L. Balch, Y.-W. Chan, R.-J. Cheng, G. N. La Mar, L. Latos-Grazynski, M. W. Renner, *J. Am. Chem. Soc.* **1984**, *106*, 7779–7785; c) R. H. Holm, *Chem. Rev.* **1987**, *87*, 1401–1449; d) C. V. Sastri, K. Oh, Y. L. Lee, M. S. Seo, W. Shin, W. Nam, *Angew. Chem.* **2006**, *118*, 4096–4099; *Angew. Chem. Int. Ed.* **2006**, *45*, 3992–3995.
[19] E. E. Chufán, C. N. Verani, S. C. Puiu, E. Rentschier, U. Schatzschneider, C. Incarvito, A. L. Rheingold, K. D. Karlin, *Inorg. Chem.* **2007**, *46*, 3017–3026.

[20] T. C. Brunold, N. Tamura, N. Kitajima, Y. Moro-oka, E. I. Solomon, *J. Am. Chem. Soc.* **1998**, *120*, 5674–5690.
[21] D. E. Bacelo, R. C. Binning, Jr., *Inorg. Chem.* **2006**, *45*, 10263–10269.
[22] a) P. E. M. Siegbahn, R. H. Crabtree, P. Nordlund, *J. Biol. Inorg. Chem.* **1998**, *3*, 314–317; b) P. E. M. Siegbahn, *Inorg. Chem.* **1999**, *38*, 2880–2889; c) P. E. M. Siegbahn, *J. Biol. Inorg. Chem.* **2001**, *6*, 27–45; d) P. E. M. Siegbahn, *Chem. Phys. Lett.* **2002**, *351*, 311–318.
[23] P. E. M. Siegbahn, L. Eriksson, F. Himo, M. Pavlov, *J. Phys. Chem. B* **1998**, *102*, 10622–10629.
[24] a) K. Yoshizawa, T. Yumura, *Chem. Eur. J.* **2003**, *9*, 2347–2358; b) T. Yumura, K. Yoshizawa, *Bull. Chem. Soc. Jpn.* **2004**, *77*, 1305–1311.
[25] See for example, a) S. Shaik, D. Kumar, S. P. de Visser, A. Altun, W. Thiel, *Chem. Rev.* **2005**, *105*, 2279–2328; b) S. P. de Visser, *J. Am. Chem. Soc.* **2006**, *128*, 9813–9824; c) S. P. de Visser, *J. Am. Chem. Soc.* **2006**, *128*, 15809–15818; d) S. Aluri, S. P. de Visser, *J. Am. Chem. Soc.* **2007**, *129*, 14846–14847.
[26] S. P. de Visser, *Angew. Chem.* **2006**, *118*, 1822–1825; *Angew. Chem. Int. Ed.* **2006**, *45*, 1790–1793.
[27] a) D. Kumar, S. P. de Visser, P. K. Sharma, E. Derat, S. Shaik, *J. Biol. Inorg. Chem.* **2005**, *10*, 181–189; b) S. P. de Visser, *J. Biol. Inorg. Chem.* **2006**, *11*, 168–178; c) S. P. de Visser, *Chem. Commun.* **2007**, 171–173.
[28] S. Shaik, S. P. de Visser, F. Ogliaro, H. Schwarz, D. Schröder, *Curr. Opin. Chem. Biol.* **2002**, *6*, 556–567.
[29] a) D. Kumar, S. P. de Visser, P. K. Sharma, S. Cohen, S. Shaik, *J. Am. Chem. Soc.* **2004**, *126*, 1907–1920; b) S. P. de Visser, D. Kumar, S. Cohen, R. Shacham, S. Shaik, *J. Am. Chem. Soc.* **2004**, *126*, 8362–8363.
[30] L. Que, Jr., *J. Biol. Inorg. Chem.* **2004**, *9*, 684–690.
[31] a) S. P. de Visser, F. Ogliaro, S. Shaik, *Angew. Chem.* **2001**, *113*, 2955–2958; *Angew. Chem. Int. Ed.* **2001**, *40*, 2871–2874; b) D. Kumar, S. P. de Visser, S. Shaik, *Chem. Eur. J.* **2005**, *11*, 2825–2835.
[32] a) S. P. de Visser, F. Ogliaro, P. K. Sharma, S. Shaik, *Angew. Chem.* **2002**, *114*, 2027–2031; *Angew. Chem. Int. Ed.* **2002**, *41*, 1947–1951; b) S. P. de Visser, F. Ogliaro, P. K. Sharma, S. Shaik, *J. Am. Chem. Soc.* **2002**, *124*, 11809–11826.
[33] F. Ogliaro, S. P. de Visser, S. Cohen, P. K. Sharma, S. Shaik, *J. Am. Chem. Soc.* **2002**, *124*, 2806–2817.
[34] a) A. D. Becke, *J. Chem. Phys.* **1993**, *98*, 5648–5652; b) C. Lee, W. Yang, R. G. Parr, *Phys. Rev. B* **1988**, *37*, 785–789.
[35] S. P. de Visser, K. Oh, A.-R. Han, W. Nam, *Inorg. Chem.* **2007**, *46*, 4632–4641.
[36] Jaguar 7.0, Schrödinger, LLC, Portland OR, 2003.
[37] Gaussian 03, Revision C.01, M. J. Frisch, G. W. Trucks, H. B. Schlegel, G. E. Scuseria, M. A. Robb, J. R. Cheeseman, J. A. Montgomery, Jr., T. Vreven, K. N. Kudin, J. C. Burant, J. M. Millam, S. S. Iyengar, J. Tomasi, V. Barone, B. Mennucci, M. Cossi, G. Scalmani, N. Rega, G. A. Petersson, H. Nakatsuji, M. Hada, M. Ehara, K. Toyota, R. Fukuda, J. Hasegawa, M. Ishida, T. Nakajima, Y. Honda, O. Kitao, H. Nakai, M. Klene, X. Li, J. E. Knox, H. P. Hratchian, J. B. Cross, V. Bakken, C. Adamo, J. Jaramillo, R. Gomperts, R. E. Stratmann, O. Yazyev, A. J. Austin, R. Cammi, C. Pomelli, J. W. Ochterski, P. Y. Ayala, K. Morokuma, G. A. Voth, P. Salvador, J. J. Dannenberg, V. G. Zakrzewski, S. Dapprich, A. D. Daniels, M. C. Strain, O. Farkas, D. K. Malick, A. D. Rabuck, K. Raghavachari, J. B. Foresman, J. V. Ortiz, Q. Cui, A. G. Baboul, S. Clifford, J. Cioslowski, B. B. Stefanov, G. Liu, A. Liashenko, P. Piskorz, I. Komaromi, R. L. Martin, D. J. Fox, T. Keith, M. A. Al-Laham, C. Y. Peng, A. Nanayakkara, M. Challacombe, P. M. W. Gill, B. Johnson, W. Chen, M. W. Wong, C. Gonzalez, J. A. Pople, Gaussian, Inc., Wallingford CT, **2004**.
[38] P. J. Hay, W. R. Wadt, *J. Chem. Phys.* **1985**, *82*, 299–310.
[39] a) D. Kumar, H. Hirao, L. Que, Jr., S. Shaik, *J. Am. Chem. Soc.* **2005**, *127*, 8026–8027; b) H. Hirao, D. Kumar, L. Que, Jr., S. Shaik, *J. Am. Chem. Soc.* **2006**, *128*, 8590–8606.

Received: November 16, 2007
Published online: April 2, 2008

